Comparison of high-resolution and time-resolved MRA in a rabbit model of pulmonary embolism at 1.5 and 7 Tesla

J. Mata[1], U. Bolzar[1], J. Mugler III[1], C. Schamber[1], W. Miller[1], S. Berr[1], and K. Hagspiel[1]
[1]Radiology, University of Virginia, Charlottesville, Virginia, United States

Introduction: High magnetic-field strengths potentially allow significant improvements for imaging many regions of the body due to the increase in signal-to-noise ratio (1-3), which can be traded for higher spatial resolution or shorter acquisition times. However, in the lungs, with their large number of air-tissue interfaces that result in strong localized field gradients induced by the magnetic-susceptibility differences, the use of magnetic resonance imaging at higher fields (≥ 3.0 Tesla) may be limited by the associated regional signal loss and reduced enhancement of the lung tissue and blood vessels following administration of a contrast agent, as compared to similar studies performed at 1.5 Tesla (4, 5). In this study, we evaluated the feasibility of using time-resolved and high-resolution contrast-enhanced magnetic resonance angiography (MRA) at 7 Tesla for characterizing an animal model of pulmonary embolism (PE) and compared the results with the same techniques at 1.5 Tesla. To our knowledge, we describe the first implementation and comparison of these techniques for application in the lung at a magnetic field strength as high as 7 Tesla.

Methods & Materials: Time-resolved and high-resolution MRA were performed in 11 New Zealand white rabbits (4-5 kg). Five were scanned using a 7-T Bruker ClinScan small-bore scanner and six on a 1.5-T Siemens Sonata clinical scanner. Due to the size of the animals and the small bore size of the 7-T scanner, the integrated body coil was used as the transmit/receive coil. At 1.5T, the standard birdcage head coil was used. The parameters for the pulse sequences were: (1) time-resolved MRA at 7T: TR/TE, 3.25/0.58 ms; matrix, 128x86; voxel size, 1.5x1.0x12 mm^3; (2) time-resolved MRA at 1.5T: TR/TE, 2.84/1.03 ms; matrix, 192x104; voxel, 1.6x1.1x12 mm^3; (3) high-resolution 3D MRA at 7T: TR/TE, 3.48/1.2 ms; matrix, 256x256; voxel, 0.5x0.5x1.0 mm^3; and (4) high-resolution 3D MRA at 1.5T: TR/TE, 2.84/1.03 ms, matrix, 92x192: voxel = 1.1x1.1x1.5 mm^3. All rabbits had undergone fluoroscopy-guided pulmonary artery catheterization and temporary occlusion balloon placement preceding the MR studies. The balloons were placed in one of the main branches of the pulmonary artery. Following inflation of the occlusion balloon, one dose (3 cc) of gadodiamide (Omniscan, Amersham Health Inc., Princeton, NJ) was injected via the ear vein, and time-resolved MRA followed by high-resolution MRA was performed. After this, the balloon was deflated and a new set of high-resolution MRA's was acquired. Signal-to-noise ratio (SNR) and contrast-to-noise ratio (CNR) values for the lungs, muscle and the aortic arch were calculated. The highest order pulmonary artery branches were recorded for each field strength and the diameters of the pulmonary artery branches were measured by a blinded reviewer.

Results: Occluded pulmonary arteries and associated reduction in pulmonary perfusion were detected in all rabbits and at both field strengths. The high-resolution 3D MRA generated images with a mean SNR of the lung parenchyma and mean CNR of the aorta vs. lung of 7.5 ± 3.3 and 126.7 ± 46.4, respectively, at 7T; and 8.2 ± 2.0 and 115.9 ± 55.1, respectively, at 1.5T. The SNR of the aorta and the SNR of the leg muscle were 134.2 ± 46.5 and 33.4 ± 16.4, respectively, at 7T; and 124.1 ± 56.2 and 30.6 ± 14.6, respectively, at 1.5T. Despite an echo time (TE) for the time-resolved MRA of 0.58 ms, we observed artifacts that were probably caused by susceptibility effects from the blood-tissue-air interfaces at high magnetic field. High-resolution MRA at 7T allowed visualization of the pulmonary arterial tree down to the 4^{th} order, while MRA at 1.5T only reached to the 3^{rd} order branches. The average diameters in cm for the non-occluded pulmonary vessels were 0.59 ± 0.006 (7T) and 0.61 ± 0.039 (1.5T) for the 1^{st} order vessels; 0.47 ± 0.028 (7T) and 0.47 ± 0.111 (1.5T) for the 2^{nd} order; 0.18 ± 0.026 (7T) and 0.29 ± 0.081 (1.5T) for the 3^{rd} order; and 0.08 ± 0.012 at 7T for the 4^{th} order.

Discussion: High-resolution MRA and time-resolved MRA at 7 Tesla are feasible and provide high SNR and CNR, as well high spatial resolution, compared with identical studies at 1.5 Tesla. Time-resolved MRA at 7 Tesla suffered from artifacts, likely caused by susceptibility effects which are substantially increased at very high magnetic fields. On the other hand, time-resolved MRA at 1.5 Tesla provided good spatial and temporal resolution, and were free of susceptibility-induced artifacts. The detection of the occluded pulmonary arteries was possible in all cases in this rabbit model of PE at both field strengths, and the 3D maximum-intensity-projection (MIP) images from the high-resolution MRA at 7 Tesla showed sub-millimeter details and up to the fourth order pulmonary branches, which could not be seen clearly at 1.5 Tesla.

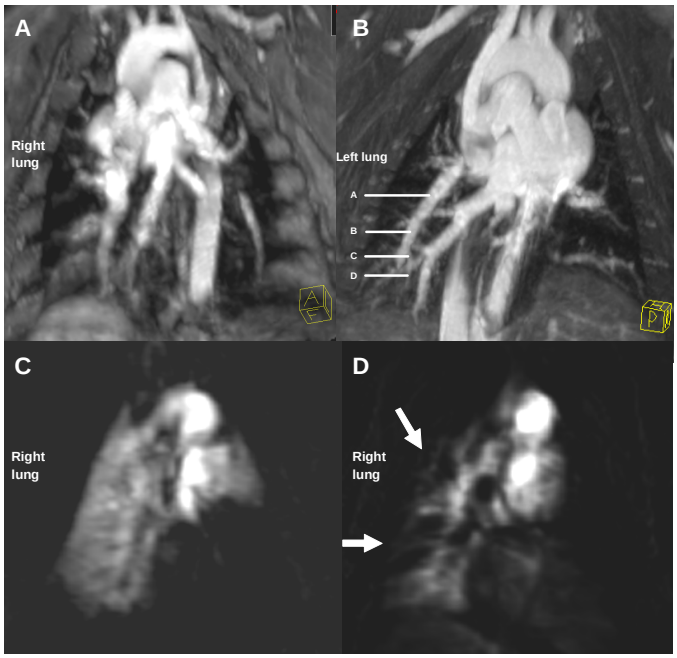

References: 1. Allkemper T, Heindel W, Kooijman H, Ebert W, Tombach B. Invest Radiol 2006;41(2):97-104.
2. von Falkenhausen MM, Lutterbey G, Morakkabati-Spitz N, Walter O, Gieseke J, Blomer R, et al.. Radiology 2006;241(1):156-166.
3. Kramer SC, Wall A, Maintz D, Bachmann R, Kugel H, Heindel W. Radiology 2004;39(7):413-417.
4. Nael K, Michaely HJ, Kramer U, Lee MH, Goldin J, Laub G, Finn JP. Radiology 2006;240(3):858-868.
5.Uematsu H, Dougherty L, Takahashi M, Ohno Y, Nakatsu M, Song HK, et al. Magn Reson Med 2001;46(5):1028-1030.

Figure 1 – A, MIP of a high-resolution MRA at 1.5 Tesla; B, MIP of a high-resolution MRA at 7 Tesla; C, time-resolved MRA of a PE lung (left lung occluded) at 1.5 Tesla; D, time-resolved MRA of a PE lung (left lung occluded) at 7 Tesla. Note the high resolution and SNR of image B, which permits clear visualization of up to the fourth-order branch of the pulmonary arteries (legend: A-D). In contrast, the spatial resolution of image A does not permit a clear delineation of the vessels above the 2^{nd}-3^{rd} order branches. Arrows on image D show the extensive artifacts presumably caused by the susceptibility effects at the 7 Tesla magnetic field.